Evaluation of cold-wire addition effect on heat input and productivity of tandem submerged arc welding for low-carbon microalloyed steels

Mohsen Mohammadijoo[1] · Laurie Collins[2] · Hani Henein[1] · Douglas G. Ivey[1,*]

[1]Department of Chemical and Materials Engineering, University of Alberta, Edmonton, AB, Canada T6G 1H9

[2]R&D Division, Evraz Inc. NA, P.O. Box 1670, Regina, SK, Canada S4P 3C7

[*]Corresponding author. Prof., Ph.D.; Tel.: +1 780 4922957; Fax: +1 780 4922881

E-mail address: divey@ualberta.ca (D.G. Ivey)

Abstract

The addition of a cold wire in conventional tandem submerged arc welding (TSAW), i.e., the CWTSAW process, is proposed to improve the productivity of pipeline manufacturing by increasing welding travel speed and deposition rate, while retaining adequate joint geometry without increasing the welding heat input. In addition to increasing productivity, incorporating a cold wire in the TSAW process improves the fracture toughness by refining the microstructure of the weld heat affected zone (HAZ). In the present work, the influence of cold-wire addition on the heat input, productivity and properties of an X70 microalloyed steel welded by CWTSAW is investigated. Charpy impact testing and microhardness testing were utilized to investigate the mechanical properties of the HAZ. Scanning electron microscopy (SEM) and tint etching optical microscopy (TEOM) were used to correlate the microstructure alterations with the properties. The low-temperature fracture toughness of the HAZ was improved by 38% when a cold wire was fed at 25.4 cm/min in the conventional TSAW process with a heat input of 22.1 kJ/cm. This improvement was attributed to a reduction in the prior austenite grain (PAG) size and martensite-austenite (M-A) constituent fraction as a result of the reduction in the effective heat input (7.5% reduction) by cold wire addition. The amount of heat input reduction is a function of the cold wire addition rate and the nominal welding heat input. The increase in travel speed and deposition rate of welding by addition of a cold wire at 58 cm/min in the TSAW process with a heat input of 23.2 kJ/cm was 26% and 12%, respectively.

Key words Microalloyed steels · Tandem submerged arc welding · Welding productivity · Heat input · HAZ toughness

1 Introduction

Due to the inherent properties of submerged arc welding (SAW), such as high deposition rate, deep penetration and capability of welding thick sections, SAW has been preferred over other welding processes to manufacture pipelines and pressure vessels [1, 2]. To improve welding productivity in a global economy, many fabricators have resorted to various techniques to increase the SAW deposition rate. The commonly used techniques to improve welding deposition rate are increasing the electrode stick-out [3], twin-wire SAW [4], tandem SAW (TSAW) [5, 6], applying a metal-cored wire [4, 7], varying electrode polarity [8] and addition of a cold-wire to a single electrode SAW [9] or in twin-wire SAW [10]. Some applications, such as pressure vessels, girth welds in pipes and spiral pipe mills, can benefit from the techniques employed to improve the deposition rate and, consequently, the productivity of the SAW process [11]. TSAW is a common process employed by industry to improve the welding deposition rate. However, in the TSAW process, heat input is increased as the number of electrodes increases because of the increase in the overall welding current and voltage to generate a higher deposition rate. Although TSAW provides higher productivity due to the high heat input, some adverse effects can be produced in terms of the microstructure, properties and geometry of the weld joint. The weld metal (WM) and particularly the heat-affected zone (HAZ) are affected by welding heat input as the weldment experiences higher peak temperatures and cools down more slowly after welding [6, 12, 13]. The addition of a cold wire to the one electrode SAW process was initially proposed by Mruczek [14]. However, it has been found that the addition of a cold wire in one electrode SAW resulted in shallower weld penetration due to the consumption of the lead electrode heat by the additional cold wire.

Tandem submerged arc welding with an additional cold-wire (CWTSAW) has been developed in our previous work [15]. The addition of a cold wire at the lagging position (close to the trail electrode) in TSAW does not reduce the penetration depth, unlike cold wire addition in SAW [14]. Since an appropriate understanding of the welding conditions is essential in the development of a welding process to guarantee requisite weld geometry, appearance and mechanical properties, the CWTSAW process was initially optimized in terms of the welding parameters (i.e., heat input, voltage and travel speed and cold wire feed speed, position and angle) and presented in [15]. The influence of cold wire addition to TSAW on the properties was also studied [16]. The coarse grain heat affected zone (CGHAZ) area and weld dilution were reduced and the mechanical properties of the HAZ were improved due to an improvement in the microstructure. These improvements, as a result of cold wire addition, were attributed to changes in the actual heat introduced to the weldment, the peak temperature and the cooling rate in the HAZ. In the current research work, a methodology for analyzing the actual heat input of the CWTSAW process is proposed and, subsequently, a detailed study on the correlation between the HAZ properties and the welding heat input is conducted. The influence of cold wire addition to TSAW on welding deposition rate and travel speed (i.e., welding productivity) is also investigated. Microstructural characterization is carried out using tint etching optical microscopy (TEOM) and scanning electron microscopy (SEM). Charpy V-notch (CVN) impact testing and microhardness testing are performed to investigate the property changes in the HAZ of samples prepared by both TSAW and CWTSAW.

2 Materials and Welding Procedure

In TSAW, the lead electrode is positioned to generate sufficient penetration depth of the weld and the trail electrode(s) provide filling of the bevel, resulting in adequate joining of the metal pieces of interest [3]. Accordingly, in the CWTSAW process, DCEP (direct current electrode positive) and ACSQ (square wave alternating current) polarities were selected for the lead and trail electrodes, respectively, since DCEP on the lead electrode causes deeper penetration and ACSQ on the trail electrode provides increased deposition rate relative to DCEP polarity. The cold wire was fed at a lagging position close to the trail electrode and consumed some of the heat of the trail electrode. Seven weld samples were prepared by CWTSAW and TSAW of 13.4±0.1 mm thick plates sectioned from X70 microalloyed steel. The geometry of the V-shaped bevel machined in the steel plates, along with the CWTSAW process set-up, are illustrated in Fig. 1. The compositions of the microalloyed steel and the consumable electrode are indicated in Table 1. The 4 mm diameter wires for the electrodes and cold wire were selected based on EN756/EN14295 (BA-S2Mo, Bavaria, Germany) and AWS A5.17/A5.23 (EA2). The BF6.5 consumable flux was chosen according to EN 760 (Bavaria, Germany).

The welding conditions to fabricate the microalloyed steel joints are presented in Table 2. Sample T1 was welded by TSAW and then compared with the welds fabricated by the CWTSAW process (i.e., samples C1-C6) in terms of productivity and properties. To determine the maximum travel speed that can be employed by cold wire addition, while maintaining adequate HAZ and weld geometry, appearance and properties, relatively high current, voltage and cold wire feed speed were employed. Visual inspection was conducted on the prepared welds prior to any further investigation to ensure that the welds were free from the macro-level defects, such as surface porosity, hot-cracking, undercutting and burn-through.

Due to the bulbous shape of the weld metal and the HAZ and the relatively small size of the HAZ, it was not possible to fabricate full size Charpy specimens of the HAZ. As such, subsize Charpy-V-notch (CVN) specimens (5 mm x 10 mm x 55 mm) were machined along the transverse welding direction according to ASTM E23-12c [17]. These were extracted as close as possible to the top metal surface to ensure that half of the notch was located in the CGHAZ and half was located in the fine grain heat affected zone (FGHAZ). In order to position the V notch in the HAZ, the specimens were firstly macro-etched with 5% Nital to outline the HAZ boundaries. Charpy impact tests were then performed at room temperature (RT), -30°C and -45°C, and at least five specimens per weld condition and test temperature were tested. To analyze the microhardness variation along the weld samples (ASTM E384 [18]), a transverse sample from each weld was extracted according to ASTM E3-11 [19] and then tested using a Wilson-VH3300 microhardness machine (Buehler, Germany). In total, forty test points were examined per weld, with an average of 14-18 indents across each of the FGHAZ and CGHAZ. Optical microscopy (Olympus BX61) and scanning electron microscopy (Tescan Vega-3 SEM) were utilized to analyze the microstructural alterations along the HAZ. Freshly polished weld specimens were then tint etched through a separate process using modified LePera's etchant [20] for 30-50 s to reveal different microstructural features. Microstructural analysis indicated a high sensitivity for phase identification to etchant composition and etching time. Quantitative analysis of the M-A constituent was done using ImageJ commercial image analysis software according to ASTM E562 [21].

3 Results and Discussion

3.1 Heat input analysis

Earlier studies done by Rigdal [22] and Mruczek [9] have reported that the addition of a cold-wire produces a heat input which is less than the nominal heat input of a conventional SAW process, since the wire absorbs heat from the weld pool and/or electrode during its melting. Given the fact that the weld/HAZ microstructure and properties are directly influenced by welding heat input, a reduction in the heat input as a result of cold wire addition causes some alteration in the microstructure and mechanical properties in the HAZ [16, 23]. The term "effective heat input" [22] has been used to describe the reduced heat input, which is based on the relative volume of the electrode and cold wire melted to produce a heat input reduction factor. Mruczek et al. [9] used hardness readings and Charpy results to verify the heat input reduction. In the present study, the Mruczek's approach is modified (Equation 1) according to the current CWTSAW process design. In our approach, it is assumed that the cold wire consumes heat of the trail electrode since the cold wire is positioned adjacent to the trail electrode. Accordingly, the cold wire solely reduces the trail electrode energy (does not affect the lead electrode); therefore, the correction factor (Equation 2) only applies to the heat input produced by the trail electrode.

$$\mathbf{HI_{eff}}\left(\frac{\mathrm{kJ}}{\mathrm{cm}}\right) = \mathrm{HI_L} + \eta.\mathrm{HI_T} = \frac{60}{1000.\mathrm{TS}}[(\mathrm{V_L}.\mathrm{I_L}) + \eta(\mathrm{V_T}.\mathrm{I_T})] \qquad (1)$$

$$\textbf{Correction factor}:\ \eta = \frac{\mathrm{Vol._T}}{\mathrm{Vol_T} + \mathrm{Vol_{CW}}} = \frac{\mathrm{FS_T}}{\mathrm{FS_T} + \mathrm{FS_{CW}}} \qquad (2)$$

where HI_{eff}, HI_L and HI_T are the effective welding heat input, lead heat input and trail heat input, respectively. Vol_T Vol_{CW} are the volumes of the electrode and cold wire melted during welding. Since the electrode and cold wire have similar diameters and chemistry in this study, the feed speed of the trail electrode (FS_T) and the cold wire (FS_{CW}) can be used to calculate the correction factor (η). For the conventional TSAW process (without additional cold wire), η is equal to 1. The WM and CGHAZ microhardness, CVN results and prior austenite grain (PAG) size were analyzed to investigate the CWTSAW heat input. For this reason, two weld samples were prepared using CWTSAW (R1 and R3) and the correction factor was calculated for each weld and applied to the heat input equation to evaluate the effective heat input of the CWTSAW process. Subsequently, the calculated effective heat input was used to prepare two weld samples by conventional TSAW (R2 and R4). Various welding parameter configurations were employed to verify the correction factor in Equation 1, as shown in Table 3. The trail electrode feed speeds for the R1 and R3 welds were measured at 201 and 212 cm/min, respectively. Accordingly, the η values for the R1 and R3 samples were calculated as 0.80 and 0.73, respectively, which means 20% and 27% of the trail electrode heat was consumed by the cold wire. As such, the effective heat input employed to prepare the R2 and R4 samples (without a cold wire addition) were 20.0 and 20.7 kJ/cm, respectively.

Table 4 shows the CVN results, average microhardness values and PAG size for weld specimens R1-R4. As indicated, the measured properties for the R2 are similar to those for the R1 and, likewise, the measured properties for R4 are similar to those for R3, respectively. These results confirm that the effective heat input of the CWTSAW process is as a function of the trail electrode and cold wire feed speed and can be accounted for by the correction factor η.

In addition to the electrode/cold-wire relative volume method for the effective heat input assessment, a heat balance analysis is also conducted to approximate the portion of the heat loss in the CWTSAW process as a result of the cold wire addition relative to the conventional TSAW process. Our experimental observations show that addition of a cold wire in the TSAW process has a two-fold effect on the reduction in the heat introduced to the weldment. When the cold wire is fed into the weld puddle/electrode arc, it consumes some portion of the weld heat to be melted ($\Delta H_{Fusion\text{-}CW}$) (Equation 3). During welding runs, the current and voltage of electrodes were recorded every 0.5 s to ensure that the recorded values are equal to the nominal values, which were initially set. However, the data recorded during the welding runs indicate that the additional cold wire slightly influenced the arc stability of the electrodes, particularly the trail electrode. As such, the average values of recorded current and voltage for the electrodes were slightly reduced compared with the nominal values, resulting in an overall reduction in the welding heat input. No significant reduction in the current and voltage of the TSAW runs was observed. This reduction is calculated based on Equation 4 ($\Delta H_{Arc\text{-}instability}$). Our observations show that the amount of reduction in the electrode current and voltage increased as the cold wire feed speed increased. Equations 5 and 6 represent the heat input correction factor (η) and the effective heat input calculated from the heat balance analysis done for the CWTSAW process, respectively. In this method, the correction factor applies to the nominal heat input of both lead and trail electrodes.

$$\Delta\mathbf{H}_{\mathbf{Fusion-CW}}\left(\frac{\mathrm{kJ}}{\mathrm{cm}}\right)=\frac{\mathrm{FS.A.\rho}}{1000.\mathrm{TS}}.\left\{\Delta\mathrm{H}_{298}^{\mathrm{o}}+\int_{25+273}^{1510+273}\mathrm{C}_{\mathrm{p}}^{\mathrm{s}}.\mathrm{dT}+\Delta\mathrm{H}_{\mathrm{l}}+\int_{1510+273}^{1900+273}\mathrm{C}_{\mathrm{p}}^{\mathrm{l}}.\mathrm{dT}\right\} \tag{3}$$

$$\Delta\mathbf{H}_{\mathbf{Arc-instability}}\left(\frac{\mathrm{kJ}}{\mathrm{cm}}\right)=\frac{60}{1000.\mathrm{TS}}.\{[(\mathrm{V_L}.\mathrm{I_L})+(\mathrm{V_T}.\mathrm{I_T})]_{\mathrm{nominal}}-[(\mathrm{V_L}.\mathrm{I_L})+(\mathrm{V_T}.\mathrm{I_T})]_{\mathrm{recorded}}\} \tag{4}$$

$$\mathbf{Correction\ factor}:\ \eta=1-\frac{\Delta\mathrm{H}_{\mathrm{Fusion-CW}}+\Delta\mathrm{H}_{\mathrm{Arc-instability}}}{\mathrm{HI}_{\mathrm{Welding}}} \tag{5}$$

$$\mathbf{HI}_{\mathbf{eff.}}\left(\frac{\mathrm{kJ}}{\mathrm{cm}}\right)=\eta.\mathrm{HI}_{\mathrm{Welding}} \tag{6}$$

where *A*, *ρ* and *TS* are the cold wire cross-section area and density and welding travel speed, respectively, and C_p^s and C_p^l are the specific heat capacities of the solid and molten wire. ΔH_l is the latent heat of fusion for the cold wire. The physical properties of the cold wire were assumed to be similar to those of a structural steel [24]. The recorded values of *I* and *V* represent the changes in the electrode current and voltage as a result of slight instability in the arc, due to the addition of a cold wire during CWTSAW. $HI_{welding}$ is the nominal welding heat input calculated according to the initial set of current and voltage used to conduct the welding process. The variation in arc current and voltage, along with the electrode characteristics, are indicated in Table 5. According to Equation 5 and 6, the correction factor, η, for the R1 and R3 weld samples is calculated as 0.92 and 0.88, respectively, which means that the nominal welding heat input is reduced by 8% and 12% by the additional cold wire. Accordingly, the CWTSAW effective heat input for R1 and R3 weld samples is 20.4 and 21.0 kJ/cm, respectively.

Table 6 indicates the η values and the effective heat input for the R1 and R3 weld samples calculated using both methods. As discussed earlier, the η value calculated from the relative volume method only applies to the trail electrode heat input, whereas the η value calculated from the heat balance analysis is employed for the entire nominal welding heat input. As such, both heat input analysis methods were in a good agreement, giving similar reductions in the nominal welding heat input by cold wire addition. The heat input analysis also confirms that cold wire addition lowers the welding heat input. However, the percentage of the heat input reduction in the CWTSAW process is a function of the cold wire feed rate.

To study the improvement of the HAZ toughness by the cold wire addition, initially three weld samples, T1, C1 and C2, were prepared (with an increase in the welding travel speed and productivity). According to the properties discussed in next section, the C1 sample showed an improvement in mechanical properties, whereas no improvement for the C2 sample (with additional cold wire) was observed relative to the T1 sample. The cold wire in the C1 sample had desirable effects on welding heat input and, consequently, cooling rate, which resulted in property improvement; however, the heat input was significantly decreased for the C2 sample, which resulted in a faster cooling rate and, therefore, no improvement in HAZ toughness. The microstructure and mechanical property changes are discussed in the next sub-sections. The relative volume method was used to calculate the effective welding heat input and the heat input analysis results were employed to prepare the C3-C6 weld samples (Table 2) to investigate welding productivity improvement by cold wire addition to the conventional TSAW process (CWTSAW).

3.2 Mechanical properties

To evaluate the mechanical property changes in the HAZ when a cold wire was added to the TSAW process, weld specimens prepared by CWTSAW (C1-C6 – Table 2) were subjected to impact testing (CVN) and microhardness analysis. Figure 2 depicts the CVN results for the HAZ of the weld samples.

The impact toughness of the C1 sample was increased when a cold wire was fed at 25.4 cm/min compared with the T1 sample at the same welding heat input. This improvement is attributed to the formation of a lower fraction of finely distributed martensite-austenite (M-A) constituents in the CGHAZ. However, the Charpy impact toughness value for the HAZ of the C2 weld was slightly reduced, relative to the T1 sample. This reduction in toughness is attributed to the formation of slender shaped M-A constituents, which formed mostly along the PAG boundaries as a result of the faster cooling rate in the CGHAZ of the C2 sample due to faster cold wire addition and lower nominal welding heat input. The microstructural alterations in the CGHAZ of the weld samples are discussed in detail in the next subsection. Given that the mechanical properties of welded microalloyed steels are directly influenced by the heat input of the welding process, the actual heat introduced to the C1 sample was calculated (according to the methods discussed in the previous subsection) and, accordingly, weld samples C3-C6 were prepared. By taking into account the heat input correction factor, η, for the C1 sample, the actual welding heat input of the C1 sample was calculated (using relative volume method) as 20.62 kJ/cm. Since the actual welding heat input of the C1 sample (due to the cold wire addition) resulted in a beneficial effect on the HAZ toughness compared with the T1 sample, the nominal welding heat input and the cold wire addition rate used to prepare the C3 to C6 weld samples were essentially selected to achieve the same actual welding heat input as for the C1 sample. Accordingly, the HAZ toughness of C3 and C4 weld samples (with higher nominal heat inputs and higher cold wire feed rates) was slightly increased relative to the T1 sample.

Although the actual welding heat inputs for the C5 and C6 weld samples were the same as for the C1 sample, a significant reduction in the toughness of the C5 and C6 weld samples was observed. Macro and microstructural investigation indicated the formation of relatively large weld defects along the fusion line, which led to deviation of the crack during testing and a brittle response for the C5 and C6 welds. The granular flux used to shield the arcs during welding was entrapped in the weld metal along the fusion line. The phenomenon of flux entrapping in the weld metal is attributed to the arc force produced during welding. Rokhlin et al. [25] have found that the arc force is directly proportional to the arc current. This phenomenon is also confirmed through the work done by Adonyi et al. [26]. Electrical current flow generates magnetic fields that interact with current carriers and produces body Lorentz forces. Halmoy [27] formulated a simple approximate relation between arc force and current from the magnetohydrodynamic theory of an ideal conducting liquid with a homogeneous distribution of current across the arc. However, this model does not take into account the arc shape during welding. A welding arc force model was developed by Converti [28] using a cone geometry, which is a better approximation to the real arc shape. The conical shape is caused by the constriction of the current at the cathode and arc expansion at the anode. The arc expansion is related to the welding current distribution and, therefore, to the arc force. According to his model, arc force has a quadratic dependence on the arc current. The relation between arc force (F_{arc}), current (I) and arc expansion (R_2/R_1) is given by Converti [28] as:

$$\mathbf{F_{arc}}: \frac{\mu_0 I^2}{8\pi}\left[1 + 2\ln\left(\frac{R_2}{R_1}\right)\right] \qquad (7)$$

where R_2 and R_1 are the radius of the arc at the base plate and at the electrode, respectively, and μ_0 is the magnetic permeability in vacuum [28]. Although the current was significantly increased for the C5 and C6 welds to increase travel speed (i.e., productivity), the arc current was not sufficient to produce enough arc force to remove all the shielding flux while welding. However, our observations indicate that increasing the arc current resulted in a negative effect on the weld properties due to an increase in the overall welding heat input as well as some welding technical challenges such as arc blowing, arc sparking and burn-through. These welding challenges as a result of high welding current are also discussed elsewhere [29]. Figure 3 depicts the formation of weld defects and x-ray microanalysis of the defects. The defect composition is a combination of Al_2O_3, MgO, SiO_2 and CaF_2, which are the components present in the shielding flux [30]. Macroanalysis of the C5 and C6 samples showed consistent formation of these defects throughout the weld.

The variation in the HAZ toughness and the microstructural alterations are attributed to changes in the actual heat introduced to the weldment and, consequently, the cooling rate in the CGHAZ, when the cold wire is added to the TSAW process. Table 7 indicates the actual welding heat input calculated according to Equation 1. It is generally accepted that cooling rate is inversely proportional to the heat input of welding; therefore, the cooling rates in the C samples are higher than that for the T1 sample, due to lower effective welding heat input of the C welds. Although the following equations developed by Easterling [31] and Poorhaydari [32] estimate the cooling rate (CR) of the weld, the equations, in this work, are employed to compare the approximate cooling times from 800 to 500ºC (Δt_{8-5}) and the cooling rates for the fabricated welds according to their effective heat inputs.

$$\Delta t_{8-5}(\text{sec}) = \frac{HI_{eff.}}{2\pi\lambda} \times \left(\frac{1}{500 - T_0} - \frac{1}{800 - T_0}\right) \quad (8)$$

$$CR\ \left(\frac{°C}{\text{sec}}\right) = \frac{300}{\Delta t_{8-5}} = \frac{2\pi\lambda(800 - T_0)(500 - T_0)}{HI_{eff.}} \quad (9)$$

where T_0 and λ are the initial temperature (25°C) and thermal conductivity (41 J s^{-1} m^{-1} $°C^{-1}$), respectively.

As shown in Table 7, the cooling rate of the C1 sample was increased by 9.5% compared with the T1 sample. The cooling rates of the C3-C6 samples were fairly close to that of C1 sample. However, due to the lower effective heat input of the C2 weld, its cooling rate was substantially increased by 21%. The variation in the welding heat input and, consequently, the cooling rate by cold wire addition governed the microstructural alterations and mechanical properties changes in the HAZ of the weld samples.

In addition to the Charpy impact testing, the weld samples were evaluated in terms of microhardness variation along the HAZ (Fig. 4). The microhardness value of the as-received microalloyed steel plate was measured as 228±4 HV. The average microhardness in the HAZ of the C1 weld was reduced when a cold wire was fed at 25.4 cm/min compared with the T1 weld. However, an increase in the microhardness for the C2 sample was observed. This is due to the lower nominal welding heat input and faster cold wire addition rate during welding, which resulted in a decrease in the effective welding heat input and, consequently, a 21% increase in the cooling rate relative to the T1 weld (Table 7). However, by proper tuning of the nominal welding heat input and cold wire addition rate in the C3 and C4 welds, resulting in an effective welding heat input the same as the C1 weld, the average microhardness in the HAZ was close to that of the C1 sample.

3.3 Welding productivity

The potential advantage of adding a cold wire in the conventional TSAW process is to increase the deposition rate to achieve a proper joint without increasing welding heat input. Moreover, to join thick sections, fewer beads are needed for a given joint, thereby increasing productivity. Given the fact that cold wire addition increases the deposition rate, ~~we have investigated~~ the possibility of the increasing welding travel speed using CWTSAW while retaining weld geometry, appearance and properties has been investigated. In this work, the T1 weld was prepared by conventional TSAW; however, a cold wire was fed during the process (i.e., C1, C3 and C4 welds) to increase the deposition rate and travel speed without property deterioration and without the use of additional heat input. Figure 5 depicts the increased travel speed and deposition rate by additional cold wire compared with the TSAW process.

3.4 Microstructure analysis

During welding, the region of the base metal affected by the heat of welding, the HAZ and the CGHAZ in particular, tends to weaken in terms of fracture toughness (relative to the base metal of the microalloyed steel) due to the high heat input and thermal cycles that the steel experiences during welding. The deterioration in toughness of the CGHAZ is essentially attributed to the formation of large PAGs and martensite-austenite (M-A) constituents, which are characterized as localized brittle zones (LBZ), as a result of the high peak temperature and relatively fast cooling rate in the CGHAZ [2, 33–36]. Davis et al. [37, 38] and Reichert et al. [39] found that the formation of a network of enlarged M-A constituents resulted in cleavage crack initiation in the HAZ. However, the fraction and size of M-A constituents are dependent on the PAG size. Yu et al. [34] and Li et al. [35] showed that the fraction of coarse M-A constituents was increased by coarsening the PAG size in the CGHAZ. They found that a coarse PAG size, associated with coarse M-A constituents, is the dominant factor in promoting brittle fracture in the CGHAZ. Gharibshahiyan et al. [40] have reported that the formation of coarser PAGs in the CGHAZ has a detrimental effect on the toughness of the HAZ. Yang and Bhadeshia [41] and Garcia-Junceda et al. [42] showed that the martensite start temperature (Ms) increased with an increase in the PAG size, which resulted in a higher volume fraction of martensite. The work done by Lee et al. [43] led to a linear relation between the martensite temperature (Ms) and the ASTM gain size number (G) for low alloy steels.

$$\boldsymbol{M_s}(^\circ\mathrm{C}) = 542.3 - 30.0 \times G \qquad (10)$$

Figure 6 indicates the variation of the Ms temperature as a function of the PAG size for T1 and C1-C4 welds. The PAG size reduction in the CGHAZ of the C welds relative to T1 weld is due to a reduction in the effective welding heat input and, consequently, a decrease in the peak temperature and an increase in the cooling rate. According to Equation (10), as the PAG size increases (the ASTM number decreases), the Ms temperature increases. The coarser PAGs in the CGHAZ of the T1 weld compared with the other weld samples resulted in a higher fraction of martensite. Furthermore, Bhadeshia [44], Yan et al. [45] and Matsuda et al. [46] have suggested that, in addition to the PAG size, cooling rate affects the morphology of the M-A constituents, which also affects the toughness of the welded steel. Kim et al. [47] have reported that M-A islands are the main metallurgical factor, which contribute to local embrittlement of microstructures of welded microalloyed steels. The Charpy impact toughness of the CGHAZ of high strength low-carbon steels is a function of the fraction, morphology, carbon content and distribution of the M-A islands. As such, there is a concurrent effect of PAG size and cooling rate on the characteristics of the transformation products, in particular the M-A constituents, in the HAZ of microalloyed steels.

To evaluate the toughness variation in the T1 and C1-C4 welds, microstructural analysis was conducted using the TEOM method [20] (Fig. 7) and SEM (Fig. 8). The microstructure in the CGHAZ of the T1 weld (with higher heat input – Fig. 7a) is comprised of polygonal ferrite (PF), granular bainite (GB), bainitic ferrite (BF) and a relatively high fraction of large M-A constituents along with large PAGs. In contrast with the T1 weld, the CGHAZ microstructure of the C1 sample is composed of finer PAGs, associated with fine, uniformly distributed M-A constituents (Fig. 7b). The characteristics and fraction of the M-A constituents formed in the CGHAZ of the C3 and C4 welds (Fig. 7d-e) are similar to those of the C1 weld, because of similar effective welding heat inputs and cooling rates. Due to the faster cooling rate in the CGHAZ of the C2 weld (with the lowest effective welding heat input), smaller PAGs were formed, resulting in a lower fraction of M-A constituents in the CGHAZ of C2. Although less M-A was formed in the CGHAZ of the C2 weld, there were more elongated M-A constituents formed along the boundaries. This may be attributed to a greater reduction in the actual heat introduced to the weldment and the relatively fast cooling rate of the C2 weld compared with the C1 and T1 welds.

The PAG size influences the phase transformation products of microalloyed steels, particularly the M-A constituents. Qiao et al. [2] and Shome [48] reported that the PAG size in the HAZ depends on the local thermal cycle and the PAG size increases when the welding heat input is increased. To evaluate the effect of M-A characteristics on the fracture toughness of the HAZ, mean size, inter-particle spacing (using the equation developed by Somekawa et al. [49]) and fraction of the M-A constituents in the CGHAZ for the T1 and C1-C4 welds were measured (Fig. 9).

As shown in Fig. 9a, the M-A fraction in the CGHAZ was reduced in the C1 and C2 samples relative to the T1 sample, as a consequence of PAG size reduction due to the lower effective welding heat input. However, the formation of slender shaped M-A constituents with large inter-particle spacing in the C2 sample, as a result of the relatively faster cooling rate, resulted in a reduction in the HAZ toughness compared with the C1 weld sample. This phenomenon has also been confirmed by the work done by Davis et al. [37], Kim et al. [47] and Lan et al. [50], who have suggested that the morphology of martensite changes and the carbon content of martensite increases in the M-A constituents as the cooling rate in the CGHAZ increases. The characteristics and fraction of M-A constituents in the CGHAZ of C3 and C4 welds were similar to those of the C1 sample; M-A was finely distributed within the PAGs with smaller inter-particle spacing relative to that of the T1 and C2 samples (Fig. 9b). According to the Charpy results and the microstructural analysis, the fracture toughness in the HAZ of C1, C3 and C4 welds was increased due to a decrease in the M-A size and inter-particle spacing in the CGHAZ. Accordingly, the formation of finely distributed M-A constituents in the CGHAZ resulted in a beneficial effect on the fracture toughness.

4 Conclusions

The addition of a cold-wire in conventional tandem submerged arc welding (TSAW), i.e., cold-wire tandem submerged arc welding (CWTSAW), has a two-fold effect on the characteristics of the welded microalloyed steels; increased welding productivity and improved properties. The additional cold wire resulted in a higher deposition rate and travel speed for welding (productivity), while retaining adequate weld appearance and properties. In this work, a 12% and

26% increase in the deposition rate and travel speed, respectively, was achieved by addition of a cold wire at 58 cm/min in the TSAW process with a heat input of 23.2 kJ/cm. Moreover, cold wire addition resulted in an overall improvement in the fracture toughness of the HAZ; however, it should be noted that the improvement is greatly influenced by the cold wire addition rate and the consequent effective welding heat input. Cold wire addition at 25.4 cm/min during TSAW with a heat input of 22.1 kJ/cm (C1 weld) showed an improvement in the fracture toughness of the HAZ due to a reduction in the PAG size and modification in the characteristics of martensite-austenite (M-A) constituents. The microstructural alterations are attributed to the lower effective welding heat input (7.5% reduction compared with the TSAW (T1) sample). The C2 weld, prepared at a lower heat input of 20.5 kJ/cm and faster cold wire addition at 63.5 cm/min relative to the C1 weld, had a smaller PAG size compared with the C1 and T1 weld samples, due to the relatively larger reduction in the effective welding heat input (17.1% reduction) and faster cooling rate in the CGHAZ of the C2 sample; however, elongated M-A constituents were formed. The relatively large elongated M-A constituents with large inter-particle spacing, which mostly formed along the boundaries in the CGHAZ, of the T1 and C2 welds compared with those of the other weld samples led to inferior toughness properties for the HAZ of the former samples, since the larger M-A constituents can stimulate the formation of microcracks leading to intergranular fracture.

Acknowledgments

The present work was financially supported by the Natural Sciences and Engineering Research Council (NSERC) of Canada, Evraz Inc. NA, TransCanada PipeLines Ltd., Enbridge Pipelines Inc., UT quality Inc. and Alliance Pipeline Ltd. Technical assistance and equipment, provided by the Research and Development Division of Evraz Inc. NA, are especially acknowledged.

References

1. Viano DM, Ahmed NU, Schumann GO, et al (2013) Influence of heat input and travel speed on microstructure and mechanical properties of double tandem submerged arc high strength low alloy steel weldments. 5:26–34. doi: 10.1179/stw.2000.5.1.26
2. Zhang YQ, Zhang HQ, Li JF, Liu WM (2009) Effect of heat input on microstructure and toughness of coarse grain heat affected zone in Nb microalloyed HSLA steels. J Iron Steel Res Int 16:73–80. doi: 10.1016/S1006-706X(10)60014-3
3. Pepin JT (2009) Effects of submerged arc weld (SAW) parameters on bead geometry and notch-toughness for X70 and X80 linepipe steels. MSc Thesis, University of Alberta
4. Fabricator (2010) Improving productivity with submerged arc welding. Fabr Manuf Assoc Intl 1–4.
5. Moeinifar S, Kokabi AH, Hosseini HRM (2011) Role of tandem submerged arc welding thermal cycles on properties of the heat affected zone in X80 microalloyed pipe line steel. J Mater Process Technol 211:368–375. doi:

10.1016/j.jmatprotec.2010.10.011

6. Kiran D V., Alam SA, De A (2013) Development of process maps in two-wire tandem submerged arc welding process of HSLA steel. J Mater Eng Perform 22:988–994. doi: 10.1007/s11665-012-0381-2
7. Thomas PD, Craig LA (1986) Automatic submerged arc welding with metal powder additions to increase productivity and maintain quality. Newport News Shipbuilding, Washington, VA
8. Pepin J, Penniston C, Henein H, et al (2012) Using semipenetration ratio to characterise effects of waveform variables on bead profile and heat affected zone with single electrode submerged arc welding. Can Metall Q 51:284–293. doi: 10.1179/1879139512Y.0000000018
9. Mruczek MF, Konkol PJ (2006) Cold wire feed submerged arc welding: Technical Report. Advanced Technology Institute (ATI), Johnstown, PA
10. ESAB (2013) Submerged arc welding (Technical Handbook). TX
11. Massey S (2012) Increasing Productivity with Submerged Arc Welding. Columbus
12. Beidokhti B, Kokabi AH, Dolati A (2014) A comprehensive study on the microstructure of high strength low alloy pipeline welds. J Alloys Compd 597:142–147. doi: 10.1016/j.jallcom.2014.01.212
13. Farhat H (2007) Effects of multiple wires and welding speed on the microstructures and properties of submerged arc welded X80 steel. PhD Diss. Univ. Saskatchewan
14. Mruczek MF, Konkol PJ (2005) Twin-arc and cold-wire-feed submerged-arc welding of HSLA-100 steel. 5th Sess. Am. Weld. Soc.
15. Mohammadijoo M, Kenny S, Collins L, et al (2016) Influence of cold-wire tandem submerged arc welding parameters on weld geometry and microhardness of microalloyed pipeline steels. Int J Adv Manuf Technol. doi: 10.1007/s00170-016-8910-z
16. Mohammadijoo M, Kenny S, Collins L, et al (2016) Effect of cold-wire addition in the TSAW process on microstructure and mechanical properties of the HAZ of X70 microalloyed pipeline steel. Am Soc Mech Eng 3:1–9. doi: 10.1115/IPC2016-64549
17. ASTM (2012) E23-12C: Standard test methods for notched bar impact testing of metallic materials. ASTM International, PA
18. ASTM (2012) E384: Standard test method for knoop and vickers hardness of materials. ASTM Int. doi: 10.1520/E0384-11E01.2
19. ASTM (2011) E3-11: Standard guide for preparation of metallographic specimens. ASTM Int. doi: 10.1520/E0003-11.2
20. LePera FS (1979) Improved etching technique for the determination of percent martensite in high-strength dual-phase steels. Metallography 12:263–268. doi: 10.1016/0026-0800(79)90041-7
21. ASTM (2011) E562-11: Standard test method for determining volume fraction by systematic manual point count. ASTM Int. doi: 10.1520/E0562-11.2
22. Rigdal S, Karlsson L, Östgren L (2002) Synergic cold wire (SCW™) submerged arc welding. ESAB Weld Cut J 57:26–31. doi: 10.1007/978-3-319-26324-3

23. Ramakrishnan M, Muthupandi V (2012) Application of submerged arc welding technology with cold wire addition for drum shell long seam butt welds of pressure vessel components. Int J Adv Manuf Technol 1–12. doi: 10.1007/s00170-012-4230-0
24. Adarsh Narang V (2005) Heat Transfer Analysis in Steel Structures. Worcester Polytechnic Institute
25. Rokhlin SI, Guu AC (1993) A Study of Arc Force , Pool Depression , and Weld Penetration During Gas Tungsten Arc Welding. Weld Res Suppl 381s–390s.
26. Adonyi Y, Richardson W, Baeslack WA (1992) Investigation of Arc Force Effects in Subsurface GTA Welding. Weld Res Suppl 321s–330s.
27. Halmoy E (1979) The pressure of the arc acting on the weld pool. Arc Physics and Weld Pool Behavior. The Welding Institute, Cambridge
28. Converti J (1981) Plasma-jets in arc welding. PhD Thesis, Massachusetts Institute of Technology
29. Connor LP, O'Brien RL (1987) Welding Handbook: Welding Technology. American Welding Society, Miami
30. Bavaria Agglomerated Welding Flux BF6.5. 1–4.
31. Easterling KE (1992) Introduction to the physical metallurgy of welding. Butterworth-Heinemann Ltd, Oxford
32. Poorhaydari K, Patchett BM, Ivey DG (2005) Estimation of Cooling Rate in the Welding of Plates with Intermediate Thickness. Weld Res 149s–155s.
33. Xia ZH, Wan XL, Tao XL, Wu KM (2012) Effect of Heat Input on Toughness of Coarse-grained Heat-affected Zone of an Ultra Low Carbon Acicular Ferrite Steel. Adv Mater Res 538–541:2003–2008. doi: 10.4028/www.scientific.net/AMR.538-541.2003
34. Yu L, Wang HH, Hou TP, et al (2014) Characteristic of martensite-austenite constituents in coarse grained heat affected zone of HSLA steel with varying Al contents. Sci Technol Weld Join 19:708–714. doi: 10.1179/1362171814Y.0000000246
35. Li X, Ma X, Subramanian SV, et al (2014) Influence of prior austenite grain size on martensite-austenite constituent and toughness in the heat affected zone of 700MPa high strength linepipe steel. Mater Sci Eng A 616:141–147. doi: 10.1016/j.msea.2014.07.100
36. Li X, Fan Y, Ma X, et al (2015) Influence of martensite-austenite constituents formed at different intercritical temperatures on toughness. Mater Des 67:457–463. doi: 10.1016/j.matdes.2014.10.028
37. Davis CL, King JE (1993) Effect of cooling rate on intercritically reheated microstructure and toughness in high strength low alloy steel. Mater Sci Technol 9:8–15.
38. Davis CL, King JE (1994) Cleavage initiation in the intercritically reheated coarse-grained heat-affected zone : Part I . Fractographic evidence. Metall Mater Trans A 25:563–573. doi: 10.1007/BF02651598
39. Reichert JM, Garcin T, Militzer M, Poole WJ (2014) A new approach using EBSD to quantitatively distinguish complex transformation products along the HAZ in X80 linepipe steel. 9th Int. Pipeline Conf.
40. Gharibshahiyan E, Honarbakhsh A, Parvin N, Rahimian M (2011) The effect of microstructure on hardness and toughness of low carbon welded steel using inert gas welding. Mater Des 32:2042–2048. doi: 10.1016/j.matdes.2010.11.056
41. Yang HS, Bhadeshia HKDH (2009) Austenite grain size and the martensite-start temperature. Scr Mater 60:493–495. doi:

10.1016/j.scriptamat.2008.11.043

42. Garcia-Junceda A, Capdevila C, Caballero FG, et al (2008) Dependence of martensite start temperature on fine austenite grain size. Scr Mater 58:134–137. doi: 10.1016/j.scriptamat.2007.09.017

43. Lee S-J, Lee Y-K (2005) Effect of Austenite Grain Size on Martensitic Transformation of a Low Alloy Steel. Mater Sci Forum 475–479:3169–3172.

44. Bhadeshia HKDH (2013) About calculating the characteristics of the martensite-austenite constituent. In: Int. Semin. Weld. High Strength Pipeline Steels. The Minerals, Metals and Materials Society, The Minerals, Metals and Materials Society (TMS), USA, pp 99–106

45. Yan P, Bhadeshia HKDH (2015) The austenite-ferrite transformation in enhanced-niobium, low-carbon steel. Mater Sci Technol 31:1066–1076. doi: DOI 10.1179/1743284714Y.0000000673

46. Matsuda F, Ikeuchi K, Fukada Y, et al (1995) Review of mechanical and metallurgical investigations of M-A constituents in welded joint in Japan.pdf. Transcations JWRI 24:1–24.

47. Kim BC, Lee S, Kim NJ, Lee DY (1991) Microstructure and local brittle zone phenomena in high-strength low-alloy steel welds. Metall Mater Trans A 22:139–149.

48. Shome M (2007) Effect of heat-input on austenite grain size in the heat-affected zone of HSLA-100 steel. Mater Sci Eng A 445–446:454–460. doi: 10.1016/j.msea.2006.09.085

49. Somekawa H, Mukai T (2006) Fracture Toughness in an Extruded ZK60 Magnesium Alloy. Mater Trans 47:995–998.

50. Lan L, Qiu C, Zhao D (2012) Analysis of martensite – austenite constituent and its effect on toughness in submerged arc welded joint of low carbon bainitic steel. J Mater Sci 47:4732–4742. doi: 10.1007/s10853-012-6346-x

Figure Captions:

Fig. 1 CWTSAW process setup: (a) Geometry of the steel plate along with the positioning of the electrodes and cold wire and (b) welding setup

Fig. 2 Charpy impact energy of the HAZ for steels welded at different travel speeds and cold wire feed rates

Fig. 3 (a) SEM secondary electron (SE) image representing defect formation in the weld region of the C5 and C6 weld samples. (b) Energy dispersive x-ray (EDX) analysis of the defect at the region indicated in the inset

Fig. 4 (a) Microhardness variation within the weld samples. (b) Average microhardness, with the standard deviation, for the FGHAZ and CGHAZ of steel samples welded by the CWTSAW and TSAW processes

Fig. 5 Percentage of increased travel speed and deposition rate as a function of the cold wire addition rate in the TSAW

Fig. 6 PAG size and Ms temperature of the CGHAZ of weld samples prepared by both CWTSAW and TSAW processes

Fig. 7 Optical micrographs of the CGHAZ of the (a) T1, (b) C1, (c) C2, (d) C3 and (e) C4 welds

Fig. 8 SEM SE images of the CGHAZ for the (a) T1, (b) C1, (c) C2 and (d) C3 samples

Fig. 9 (a) Fraction and mean size of M-A constituents in the CGHAZ and (b) M-A inter-particle spacing in the CGHAZ for the weld samples

Figures:

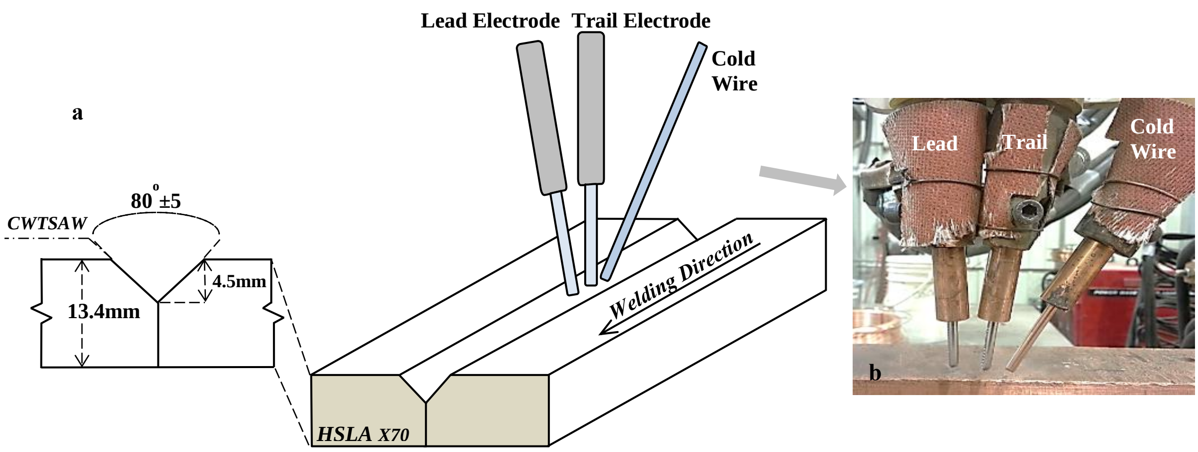

Fig. 1

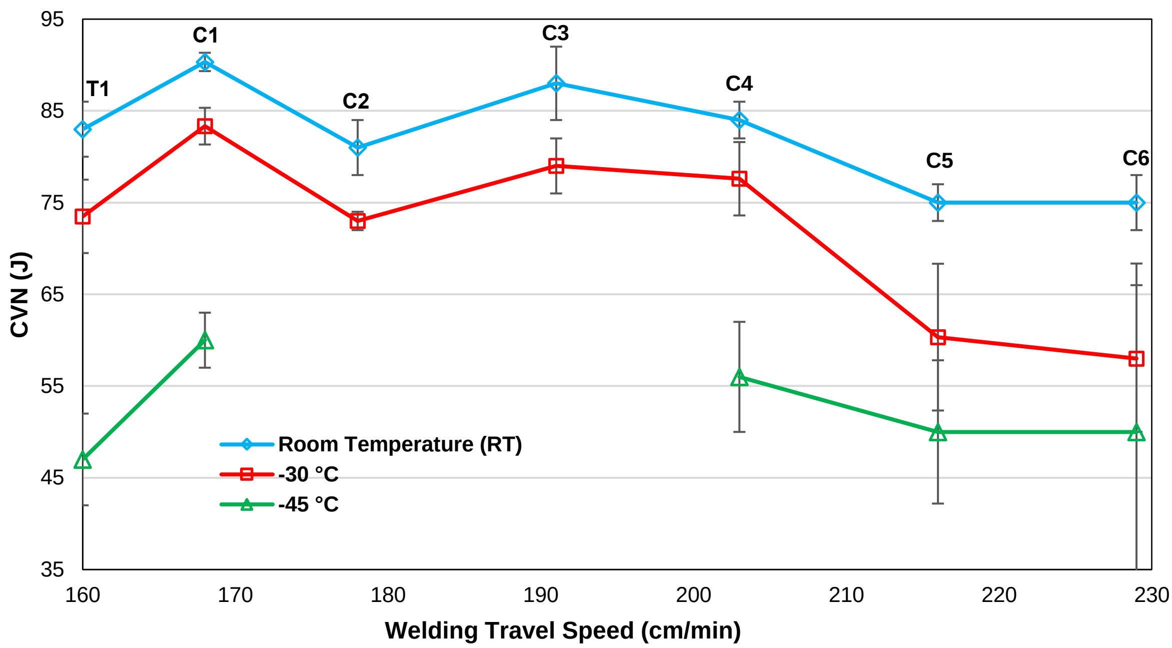

Fig. 2

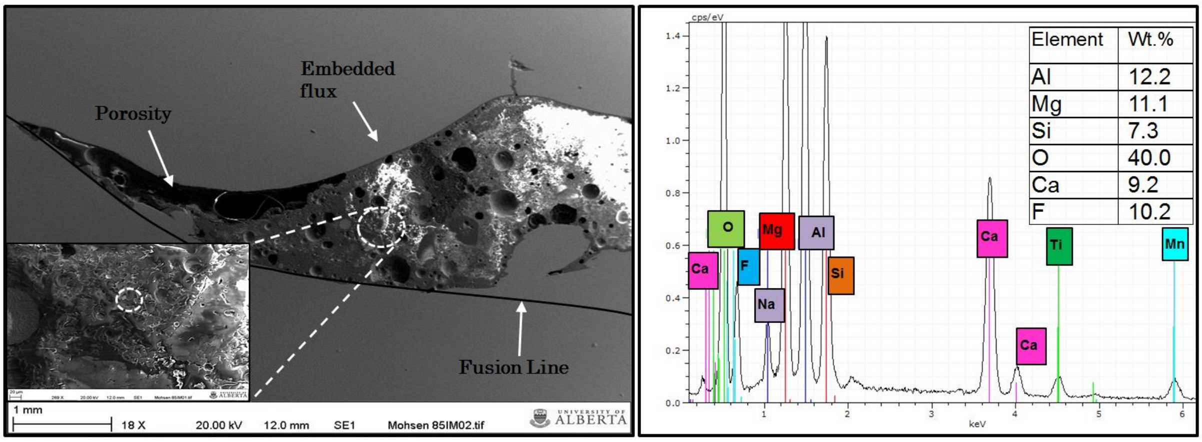
Embedded flux
Porosity
Fusion Line
1 mm
18 X
20.00 kV
12.0 mm
SE1
Mohsen 85IM02.tif
UNIVERSITY OF ALBERTA
cps/eV
Element Wt.%
Al 12.2
Mg 11.1
Si 7.3
O 40.0
Ca 9.2
F 10.2
O
Mg
Al
Ca
F
Si
Na
Ti
Mn
keV

Fig. 3

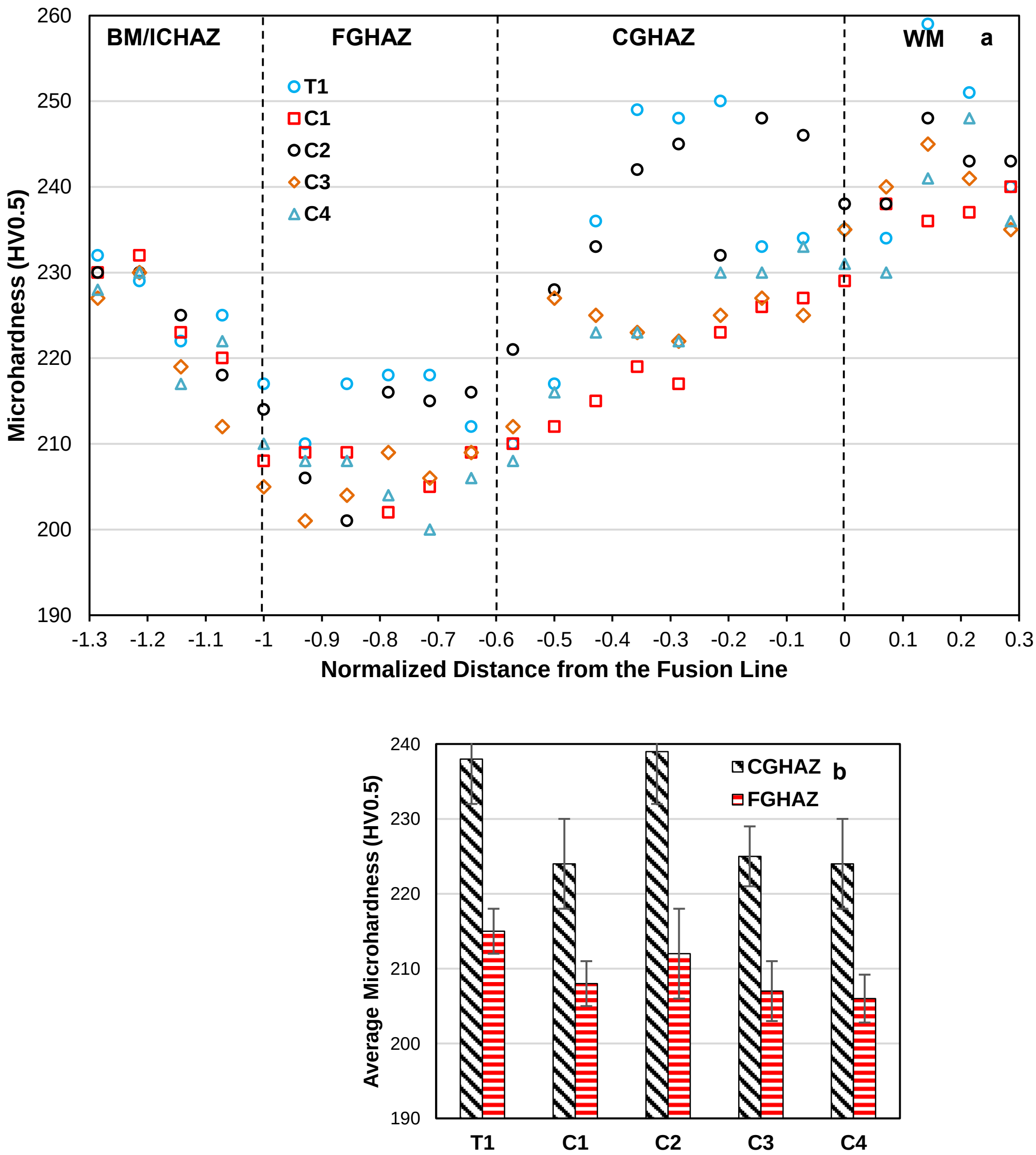
BM/ICHAZ
FGHAZ
CGHAZ
WM
a
T1
C1
C2
C3
C4
Microhardness (HV0.5)
Normalized Distance from the Fusion Line
CGHAZ
FGHAZ
b
Average Microhardness (HV0.5)
T1
C1
C2
C3
C4

Fig. 4

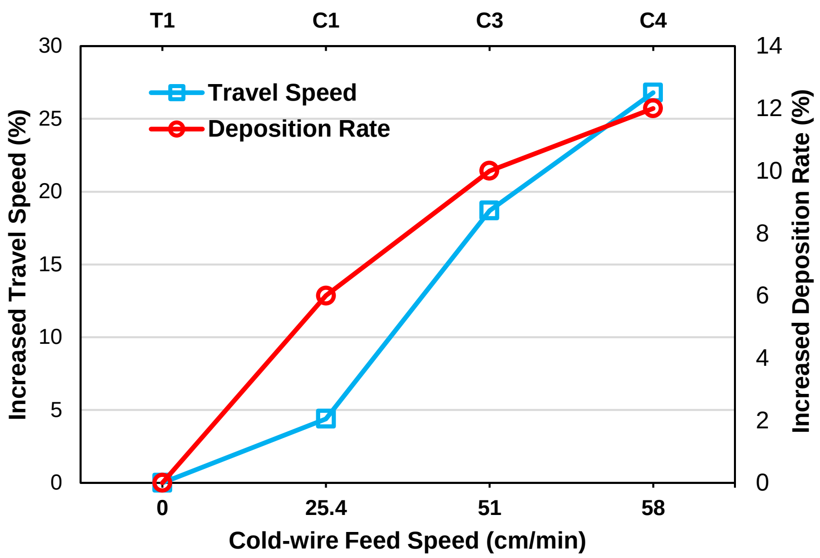
T1
C1
C3
C4
Travel Speed
Deposition Rate
Increased Travel Speed (%)
Increased Deposition Rate (%)
30
25
20
15
10
5
0
14
12
10
8
6
4
2
0
25.4
51
58
Cold-wire Feed Speed (cm/min)

Fig. 5

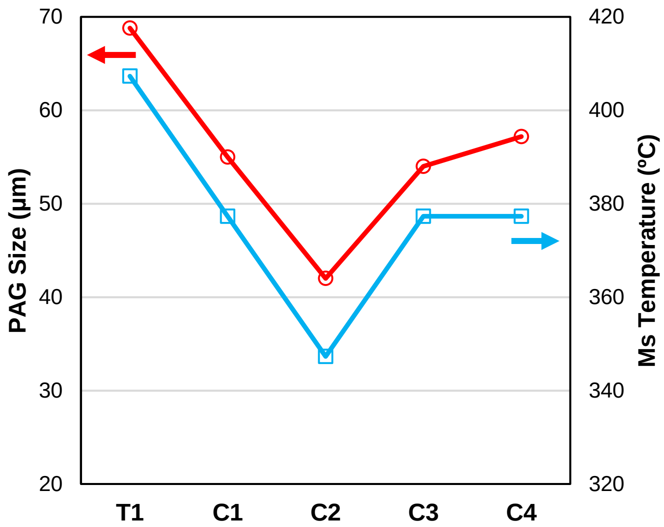
PAG Size (μm)
Ms Temperature (°C)
70
60
50
40
30
20
420
400
380
360
340
320
T1
C1
C2
C3
C4

Fig. 6

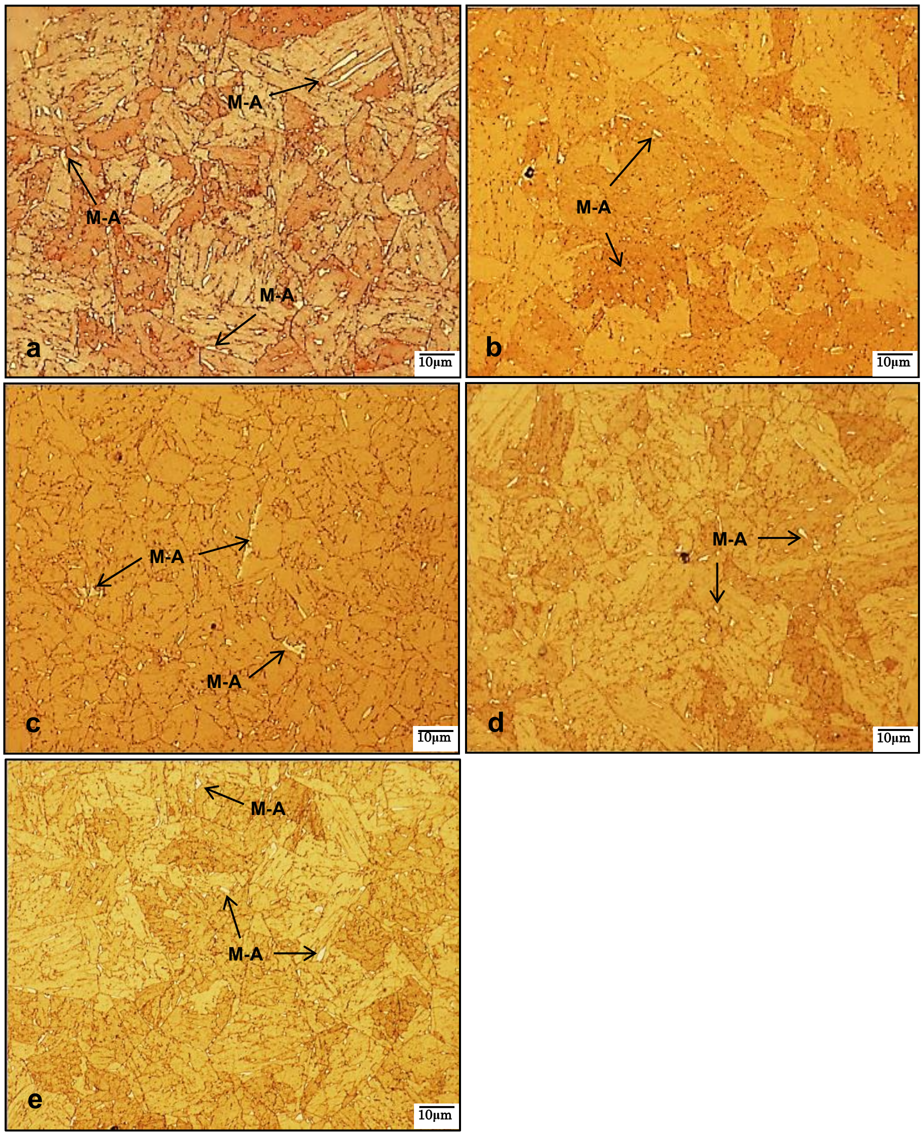

Fig. 7

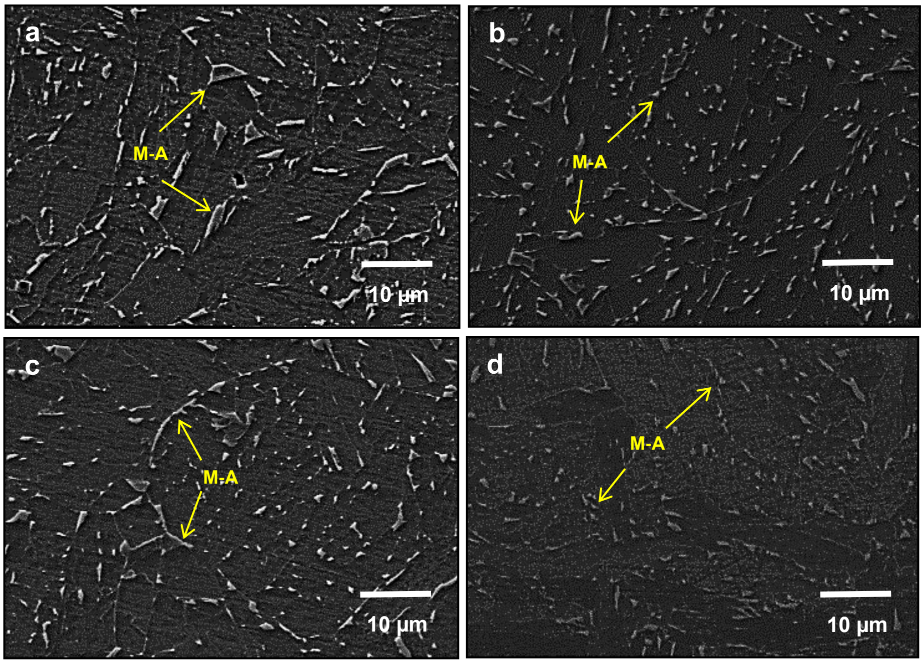
a
M-A
10 µm
b
M-A
10 µm
c
M-A
10 µm
d
M-A
10 µm

Fig. 8

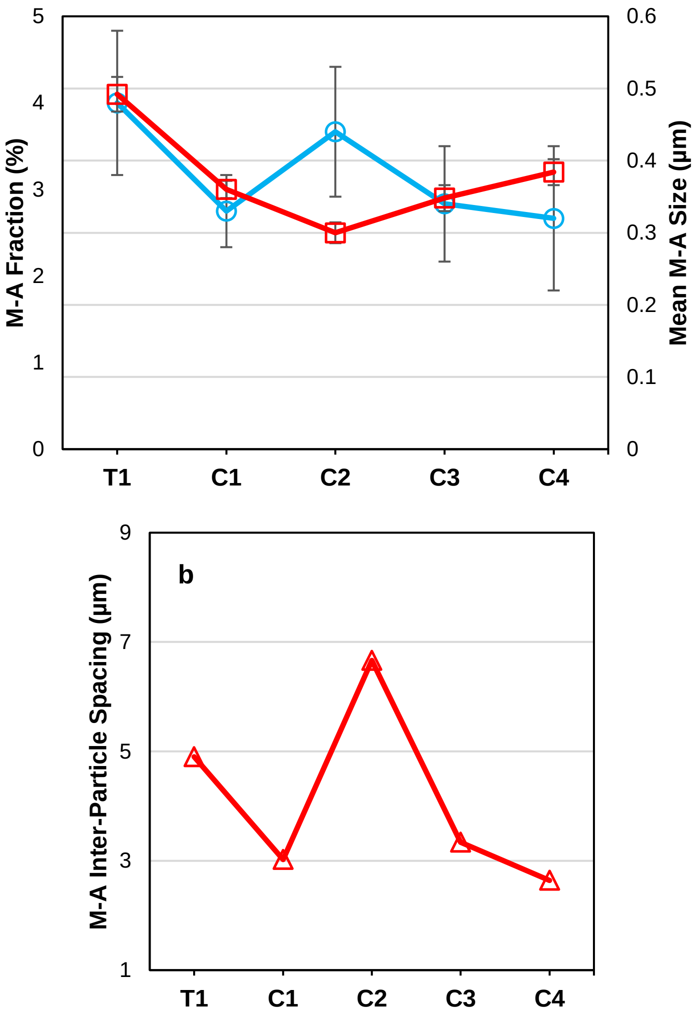
M-A Fraction (%)
Mean M-A Size (µm)
0
1
2
3
4
5
0
0.1
0.2
0.3
0.4
0.5
0.6
T1
C1
C2
C3
C4
b
M-A Inter-Particle Spacing (µm)
1
3
5
7
9
T1
C1
C2
C3
C4

Fig. 9

Table List:

Table 1 X70 microalloyed steel and electrode compositions (wt%)

X70 composition (Pcm=0.175 wt.%)							
C	**P**	**S**	**Mn**	**Si**	**N**	**V+Mo+Nb+Ti**	**Cu+Ni+Cr+Sn+Al+Ca**
0.043	0.013	0.001	1.73	0.28	0.008	0.21	0.57

Electrode and cold-wire composition (BA- S2Mo)								
C	**P**	**S**	**Mn**	**Si**	**Mo**	**Ni**	**Cr**	**Cu**
0.10	0.007	0.01	1.04	0.1	0.56	0.02	0.03	0.03

Table 2 Welding process parameters

Process Parameter		*Weld sample ID*						
	Unit	**T1**	**C1**	**C2**	**C3**	**C4**	**C5**	**C6**
Current-Lead Electrode	A	1040	1060	1070	1200	1250	1300	1350
Current-Trail Electrode	A	830	830	840	950	1000	1050	1050
Voltage-Lead Electrode	V	30	31	31	32	33	34	36
Voltage-Trail Electrode	V	34	34	34	36	37	38	39
Travel Speed	cm/min	160	167	177	190	203	216	229
Welding Heat Input	kJ/cm	22.3	22.1	20.5	23.0	23.2	23.5	23.6
Cold Wire Feed Speed	cm/min	NA	25.4	63.5	51	58	66	71

Table 3 Welding runs performed to evaluate the effective heat input for the CWTSAW process

Process Parameter			*Weld Sample ID*			
	Notation	***Unit***	**R1**	**R2**	**R3**	**R4**
Current-Lead Electrode	I_L	A	1040	980	1085	1000
Current-Trail Electrode	I_T	A	830	810	900	850
Voltage-Lead Electrode	V_L	V	30	28	30	28
Voltage-Trail Electrode	V_T	V	34	32	34	32
Travel Speed	TS	cm/min	160	160	160	160
Cold Wire Feed Speed	FS_{CW}	cm/min	50.8	NA	76.2	NA

Table 4 Measured CVN, microhardness and PAG size for R1-R4 weld specimens

Weld Sample	*Welding Process*	*Heat Input (kJ/cm)*	*CVN (J)*		*PAG Size (μm)*		*Microhardness (HV0.5)*		
			RT	*-30 ºC*	*CGHAZ*	*FGHAZ*	*CGHAZ*	*FGHAZ*	*WM*
R1	CWTSAW	22.2	86±2.3	67±7.0	50.0±5.5	4.3±0.2	226±3.6	210±1.5	238±2.5
R2	TSAW	20.0	87±4.2	67±6.1	48.5±6.3	4.2±0.3	225±3.0	208±1.0	237±4.4
R3	CWTSAW	23.7	82±4.3	60±8.0	61.4±6.0	5.1±0.5	246±3.2	219±3.6	253±6.0
R4	TSAW	20.7	80±1.5	59±7.3	59.8±4.5	4.9±0.4	240±6.5	222±2.1	256±3.2

Table 5 Welding parameters and physical characteristics of the electrodes and cold wire

Parameter	*Notation*	*R1*		*R3*	
		Set	*Recorded*	*Set*	*Recorded*
Current-Lead Electrode	I_L	1040	1039	1085	1083.5
Current-Trail Electrode	I_T	830	828.6	900	897.6
Voltage-Lead Electrode	V_L	30	29.2	30	28.6
Voltage-Trail Electrode	V_T	34	32.5	34	32
Cold-wire feed speed	FS	50.8	50.8	76.2	76.2
	ρ (kg/cm^3)	ΔH_l (kJ/kg)	C_p^s (J/kg.K)		C_p^l (J/kg.K)
Cold wire/Electrode Characteristics	$7.87*10^{-3}$	270	$425 + 0.733T + 1.69 \times 10^{-4}T^2$ (**20<T<600**) $666 \times [13002/(T - 738)]$ (**600<T<735**) $545 - [17820/(T - 731)]$ (**735<T<900**) 650 (**900<T<1510**)		820

Table 6 Effective welding heat input calculated from the relative volume method and heat balance analysis method

Weld Sample	***Heat input analysis method***	η	***Effective welding heat input (kJ/cm)***
R1	Electrode/cold-wire relative volume	0.80	20.0
	Heat balance analysis	0.92	20.4
R3	Electrode/cold-wire relative volume	0.73	20.7
	Heat balance analysis	0.88	21.0

Table 7 Calculated actual welding heat input, CR and Δt_{8-5} for the weld samples

Weld Sample	***Nominal Heat Input (kJ/cm)***	***Correction Factor (η)***	***Effective Heat Input (kJ/cm)***	***CR (ºC s^{-1})***	***Δt_{8-5} (sec)***
T1	22.3	1.00	22.30	42.0	7.1
C1	22.1	0.87	20.62	46.0	6.5
C2	20.5	0.75	18.50	52.0	5.8
C3	23.0	0.79	20.65	46.0	6.5
C4	23.2	0.78	20.72	45.8	6.5
C5	23.5	0.77	20.81	45.6	6.6
C6	23.6	0.76	20.88	45.4	6.6